Atmos. Meas. Tech. Discuss., https://doi.org/10.5194/amt-2018-229
Manuscript under review for journal Atmos. Meas. Tech.
Discussion started: 13 August 2018

Atmospheric Measurement Techniques Discussions

Comparison of Methods to Derive Radial Wind Speed from a Continuous-Wave Coherent Lidar Doppler Spectrum

Dominique P Held[1,2] and Jakob Mann[1]

[1]DTU Wind Energy, Roskilde 4000, Denmark
[2]Windar Photonics A/S, Taastrup 2630, Denmark

Correspondence: Dominique P Held (domhel@dtu.dk)

Abstract. Continuous-wave lidar systems offer the possibility to remotely sense wind speed but are also affected by inherent differences in their measurement process compared to more traditional anemometry like cup or sonic anemometers. Their large measurement volume leads to an attenuation of turbulence. In this paper we study how different methods to derive the radial wind speed from a lidar Doppler spectrum can mitigate turbulence attenuation. The centroid, median and maximum methods are compared by estimating transfer functions and calculating root mean squared errors (RMSE) between a lidar and a sonic anemometer. Numerical simulations and experimental results both indicate that the maximum method, even though using the least amount of information from the Doppler spectrum, performs best at mitigating the volume averaging effect. However, this benefit is paid by increased signal noise due to the discretisation of the maximum method. The median method shows slight improvements over the centroid method in terms of volume averaging reduction and also resulted in the overall lowest RMSE. Thus, when the aim is to obtain point-like wind speed time series with high temporal resolution, the median method is superior to the centroid and maximum method. When comparing 10 minute averages there is no difference between the methods.

1 Introduction

Remote sensing is an attractive alternative to traditional in-situ measurements of wind speed. For wind turbines, light detection and ranging (lidar) devices can replace the installation of large meteorological masts hosting cup or sonic anemometers in order to meet the constantly increasing measurement height requirements. This led to a large variety of applications spanning from lidar-assisted yaw and pitch control (Schlipf, 2015) to site assessment (Sanz Rodrigo et al., 2013) and power curve validation (Borraccino et al., 2017). However, one has to keep in mind that there is one important principal difference between measurements from a lidar device and sonic or cup anemometers, namely the averaging over a rather large measurement volume.

Continuous-wave (cw) lidars emit a laser beam focused on a desired point in space and measure the backscattered light. The radial speed of the aerosols can be estimated from the induced Doppler shift of the backscattered light. However, there exists an ambiguity in the definition of the dominant frequency of the Doppler spectrum. In the beginning, simply the maximum value of the power spectral density (PSD) was used. But since this gives integer multiples of the frequency step (which depends on the FFT setup) it has the disadvantage of returning a noisy signal. Thus, nowadays most commercial cw lidar systems

Atmos. Meas. Tech. Discuss., https://doi.org/10.5194/amt-2018-229
Manuscript under review for journal Atmos. Meas. Tech.
Discussion started: 13 August 2018

Atmospheric Measurement Techniques Discussions

use the centroid of the PSD above a certain noise level (Harris et al., 2006), while in research instruments (e.g. short-range WindScanner) the median method is implemented (Angelou et al., 2012).

For pulsed lidars, Frehlich (2013) presents an investigation on the maximum likelihood (ML) algorithm and minimum mean-squared-error method. Both estimators had similar performance and the latter was chosen because of computational efficiency. In addition Dolfi-Bouteyre et al. (2016) examined two simple methods (maximum and centroid), the previously mentioned ML approach, polynomial fitting and an adaptive filter method. The polynomial fitting method was found to perform best in laminar flow but it is suggested that in more complex flow advanced estimators are needed. For a cw lidar however these more complex methods are unavailable because they rely on an underlying model, which cannot be formulated in the case of a cw lidar.

There is a wide variety of studies investigating the correlation between lidars and sonic or cup anemometers. An early study by Lawrence et al. (1972) compared a cw carbon dioxide (CO_2) lidar to a cup anemometer around 10 m above the ground. Due to the short focus distance (approximately 30 m) the averaging volume was less than 0.5 m and both measured time series and power spectral densities showed very close agreement with no visible influence of volume averaging. A cw CO_2 lidar at focus distances up to 200 m close to the ground was used in Banakh and Smalikho (1999). Here high-frequency fluctuation attenuation due to volume averaging was observed and agreed well with theoretical predictions.

A single cw lidar focused close to a sonic anemometer mounted 78 m above ground was used in Sjöholm et al. (2009). Data gathered at 20 Hz was used to investigate the spatial averaging and good agreement between theory and signals were found for the spectral transfer function. Low-level clouds affected the measurements negatively. The same objective was followed in Angelou et al. (2012), where the transfer function of a tower-mounted horizontally staring lidar has been determined against a mast-mounted sonic anemometer allowing for horizontal measurements. The study was limited to when the lidar beam was aligned with the wind direction and these periods yielded great agreement to theory as well.

A slightly different approach was followed in Peña et al. (2017). Here a cw and pulsed nacelle lidar are compared against both a cup and sonic anemometer. Turbulence statistics were calculated by fitting a spectral tensor model including a lidar volume averaging model and an average Doppler spectrum method, which was also used in Branlard et al. (2013). The first method allowed to retrieve filtered turbulence statistics, while the second yielded unfiltered measures. Again predictions of the spatial averaging effect was consistent with theory.

The study in Borraccino et al. (2016) compared a pulsed and cw lidar to a cup anemometer for the purpose of calibration and determining uncertainties. 10 minute average radial wind speeds comparisons showed very good correlation between the two devices. Lidar uncertainties decrease with wind speed, but approximately 90% stems from the cup anemometer itself.

Two studies investigated the comparison of long-range pulsed lidar to mast-mounted sonic anemometers (Mann et al., 2009; Fuertes et al., 2014). Both studies showed the feasibility of measuring 3D wind vectors by synchronised lidars focused on one point in space. It is also shown that the attenuation from spatial averaging can be predicted by the appropriate theory. Multi-beam pulsed lidars in complex terrain were compared to sonic anemometers in Pauscher et al. (2016) and showed improved correlation to profiling lidars. However, the spatial averaging led to an underestimation of wind speed variances. No correction for the spatial averaging was used in this study.

Atmos. Meas. Tech. Discuss., https://doi.org/10.5194/amt-2018-229
Manuscript under review for journal Atmos. Meas. Tech.
Discussion started: 13 August 2018

Atmospheric Measurement Techniques Discussions

A machine-learning approach to produce unfiltered wind speed variances from pulsed lidar signals was used in Newman and Clifton (2017). Besides a model for the spatial averaging the algorithm also includes automatic noise removal. Comparisons to sonic anemometers showed improvements when using the algorithm under all stability classes but the results are highly dependent on the input variables and the training sets.

From the studies mentioned above it can be seen that the effect of the lidar's spatial averaging can be predicted theoretically, which has also been confirmed experimentally. In contrast to pulsed lidars, little work has been done on the effect of how the radial wind speed is calculated from a Doppler spectrum. Thus, the objective of this study is to investigate the influence of using different methods of determining the dominant frequency in a lidar Doppler spectrum (maximum, median, centroid) and its influence on the volume-averaging effect of lidar measurements.

2 Materials and Methods

Statistically, the fluctuating part of an incompressible, homogeneous wind field $\boldsymbol{u}(\boldsymbol{x})$ can be described by the spectral tensor $\boldsymbol{\Phi}_{ij}(\boldsymbol{k})$, where $\boldsymbol{k}$ is the wavenumber vector. To simulate synthetic wind fields, models for $\boldsymbol{\Phi}_{ij}(\boldsymbol{k})$ have been derived, e.g. von Karman (1948) or Mann (1994). This allows on one hand to directly calculate the statistical behaviour of a point measurement (sonic) and a volume measurement (lidar) in wave number space and on the other hand to generate a turbulence box and calculate Doppler spectra from which the radial wind speed can be derived. Both methods will be compared to the experimental findings.

2.1 Theory

A cw lidar measurement can be modelled by the convolution between the projected radial component $\boldsymbol{n} \cdot \boldsymbol{u}$ and a weighting function $\varphi(s) = \frac{1}{\pi} \frac{z_R}{z_R^2 + s^2}$ (Sonnenschein and Horrigan, 1971):

$$v_r(\boldsymbol{r}) = \int_{-\infty}^{+\infty} \varphi(s) \boldsymbol{n} \cdot \boldsymbol{u}(s\boldsymbol{n} + \boldsymbol{r}) ds, \tag{1}$$

where z_R is the so-called Rayleigh length, s is the distance from the focus point along the beam, $\boldsymbol{n}$ is the beam unit vector and $\boldsymbol{r}$ is the focus position. This is the definition of the centroid of the Doppler spectrum; in the following we will refer to it as *cen*. Another method of determining the dominant frequency in a Doppler spectrum is the by simply taking the frequency bin where the peak occurs (*max*) or by treating it as a PDF and taking the median value (*med*). The estimated of the radial wind speed using these three methods will be compared to the laser line projected sonic wind velocity $v_s = \boldsymbol{n} \cdot \boldsymbol{u}(\boldsymbol{x})$.

To evaluate the how well lidar and sonic measurements correlate in wave number domain an estimation of the transfer function between the two signals is used:

$$G(k_1) = \left| \frac{\chi_{r,s}(k_1)}{F_s(k_1)} \right|^2, \tag{2}$$

Atmos. Meas. Tech. Discuss., https://doi.org/10.5194/amt-2018-229
Manuscript under review for journal Atmos. Meas. Tech.
Discussion started: 13 August 2018

Atmospheric Measurement Techniques Discussions

where $\chi_{r,s}(k_1)$ refers to the cross-spectrum between the lidar and sonic signal and $F_s(k_1)$ refers to the auto-spectrum of the sonic signal. The closer $G(k_1)$ is to unity, the smaller the effect of volume averaging of the lidar is. We prefer to use the transfer function defined in eq. 2 to the more traditional $G(k_1) = F_r(k_1)/F_s(k_1)$ because the auto-spectrum $F_r(k_1)$ may be affected by noise whereas the cross-spectrum $\chi_{r,s}(k_1)$ is not (Angelou et al., 2012) assuming the sonic time series to be noiseless.

When using $\mathcal{F}[\varphi(s)](k) = \exp(-z_R|k|)$, eq. 1 can be expressed in wave number space by

$$F_r(k_1) = \int_{-\infty}^{+\infty}\int_{-\infty}^{+\infty} \mathbf{\Phi}_{ij}(\boldsymbol{k}) \exp\left(-2z_R|\boldsymbol{n}\cdot\boldsymbol{k}|\right) dk_2 dk_3, \tag{3}$$

where $\mathcal{F}[.]$ refers to the Fourier transformation. The integration in eq. 3 can be solved analytically only for simple forms of $\mathbf{\Phi}_{ij}(\boldsymbol{k})$. For the line-of-sight projected sonic measurement v_s, which can be approximated by a point measurement due to the small volume measurement, the exponential term in eq. 3 drops out and we are left with

$$F_s(k_1) = \int_{-\infty}^{+\infty}\int_{-\infty}^{+\infty} \mathbf{\Phi}_{ij}(\boldsymbol{k}) dk_2 dk_3. \tag{4}$$

The cross spectrum between the lidar and sonic measurements can then be written as

$$\chi_{r,s}(k_1) = \int_{-\infty}^{+\infty}\int_{-\infty}^{+\infty} \mathbf{\Phi}_{ij}(\boldsymbol{k}) \exp\left(-z_R|\boldsymbol{n}\cdot\boldsymbol{k}|\right) dk_2 dk_3, \tag{5}$$

It should be noted that $\lim_{k_1\to 0} G(k_1) = 1$ is only true when the lidar beam is aligned with the mean wind direction. In misaligned cases $\lim_{k_1\to 0} G(k_1) < 1$ holds (Kristensen and Jensen, 1979).

Another measure used to evaluate the performance of the different methods is the root mean squared error (RMSE)

$$\mathrm{RMSE}(v_{r,\mathrm{method}}) = \sqrt{\overline{(v_{r,\mathrm{method}} - v_s)^2}}, \tag{6}$$

where method refers to either centroid, median or maximum and the over-bar indicates averaging. In contrast to the transfer function estimate mentioned previously, for this measure the signal noise in lidar measurements will affect the performance and gives an indication of the difference between lidar and sonic measurements in time domain.

2.2 Numerical Simulations

Numerical simulations illustrate results in an environment where no noise is present. Similar simulations have also been used in Mann et al. (2010). First it is described how a Doppler spectrum is obtained from a simulated wind time series. We narrowed our investigation to the (horizontal) 2D case where the cw lidar is measuring horizontally only. We furthermore assumed Taylor's frozen turbulence hypothesis:

$$\boldsymbol{u}(x, y, t = 0) = \boldsymbol{u}(x + Ut, y, t), \tag{7}$$

Atmos. Meas. Tech. Discuss., https://doi.org/10.5194/amt-2018-229
Manuscript under review for journal Atmos. Meas. Tech.
Discussion started: 13 August 2018

Atmospheric Measurement Techniques Discussions

where U is the mean wind speed, so the wind field at any given time can be obtained by translating the wind field at $t = 0$. We did not consider any sources of noise. In this case the Doppler spectrum $S(v,t)$ can be written as:

$$S(v,t) = \int_{-\infty}^{\infty} \varphi(s)\delta(v - \boldsymbol{u}(s)\cdot\boldsymbol{n})ds, \tag{8}$$

where δ is the Dirac delta function. Notice that (8) is a convolution of the weighting function φ and the delta function $\delta(v - \boldsymbol{u}\cdot\boldsymbol{n})$). If φ was disregarded, equation (8) could be viewed as a histogram of wind velocities. The discretization of the histogram is chosen to match the typical velocity bin resolution, which in this simulation case was 0.1 ms/bin. When φ is included, the wind velocities are weighted, such that the velocities around the focus point count most. Due to the finite length of the simulated turbulent boxes the integration in eq. 8 needs to be truncated. Here we chose a distance of $M = 12z_R$ along the beam after which the truncation is applied, where the Lorentzian weighting function has a value of $\approx 1.5 \cdot 10^{-4}$ (or 0.69% relative to the maximum value at the focus point)

$$S(v,t) = \int_{-M}^{M} \varphi(s)\delta(v - \boldsymbol{u}(s)\cdot\boldsymbol{n})ds. \tag{9}$$

To generate the wind time series we assumed for simplicity that the turbulent fluctuations in the direction of the mean wind can be described by the model by Mann (1994)[1]. A turbulent wind box was created with a 2D wind vector at each grid point. The dimensions of the box are 4096×4096 grid points with a separation of 0.732 m. A total of 20 turbulent boxes with different initial turbulence seed have been simulated. Note that here we only simulate the fluctuating part and the mean wind speed is zero. An illustration of the simulation setup and an example of a simulated Doppler spectrum including the radial wind speed estimates using the three different methods is shown in fig. 1.

2.3 Experimental Setup

In this section the experiment conducted at Risø campus with a lidar system by Windar Photonics A/S will be presented. The *WindEYE* is a commercial Doppler wind lidar that uses an all-semiconductor laser source with a wavelength of 1553 nm, see Hu (2016). Because the purpose of the product is wind direction measurement, it can focus at two positions by deflecting the beam through two different lenses. The switching occurs every half second, which means that the lidar focuses on one position for 0.5 s and then a liquid crystal will bend the beam towards the second focus point for another 0.5 s. Usually the device is mounted on the nacelle of wind turbines, but for this experiment it was installed on a tower to be able to focus at the location of two sonic anemometers around 10 m above the ground, see fig 2. The focus distance is 90 m and Rayleigh length $z_R = 14.5$ m. The angle between the two beams is 30°, but since the beams are compared individually it is of no importance here.

The sonic anemometers are two USA-1 anemometers by Metek GmbH, which were mounted on a tower at the exact position of the focus points. The focus distances have been verified experimentally in an optical laboratory and the alignment of the lidar to the sonic anemometers have been checked using an infrared sensor card, see Dellwik et al. (2015). The sonic anemometers

[1]The software can be downloaded free of charge at http://www.wasp.dk/weng#details__iec-turbulence-simulator

Atmos. Meas. Tech. Discuss., https://doi.org/10.5194/amt-2018-229
Manuscript under review for journal Atmos. Meas. Tech.
Discussion started: 13 August 2018

Atmospheric Measurement Techniques Discussions

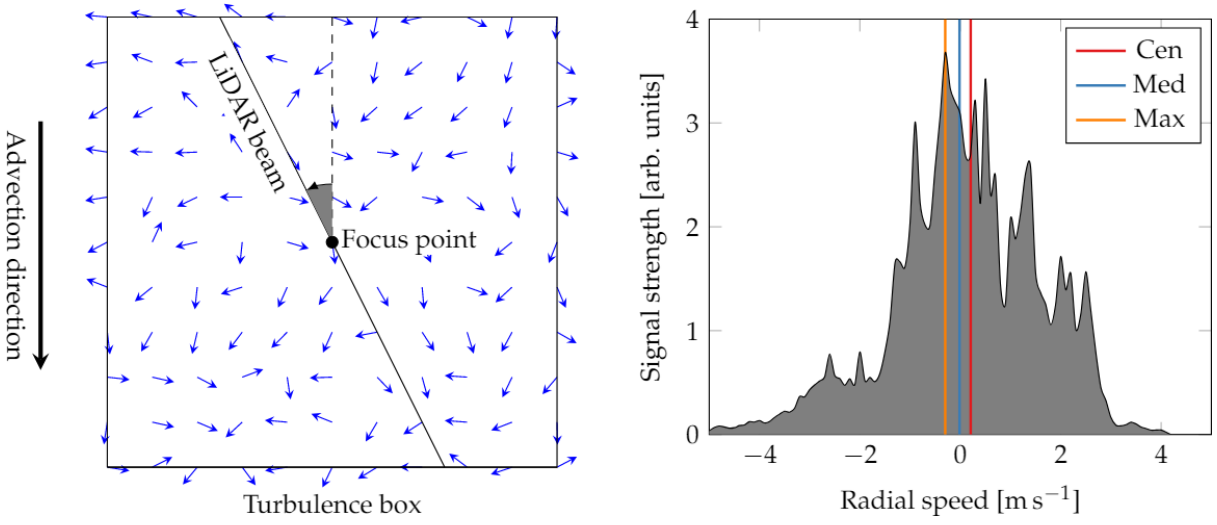

Figure 1. *Left:* Illustration of the lidar simulation setup. *Right:* Example of an instantaneous Doppler spectrum, where the radial wind speed has been determined by the three different methods.

were sampling at 35 Hz and have a transducer distance of 0.175 m implying that the device (compared to the averaging volume of the lidar) is close to perform a point measurement. For all measurements the standard 2-D flow correction has been removed and instead a 3-D correction was used (Bechmann et al., 2009). Due to the inherent switch mechanism of the WindEYE lidar the data had to be combined to a rather low sampling frequency of 1 Hz. The experiment extended from January 9$^{\text{th}}$ to March 23$^{\text{rd}}$ 2014 but due to synchronization problems only the periods in February and March could be used.

3 Results and Discussion

In this section we first present an example of the numerical simulation and experimental results and then we will compare both to the analytical results. An example of the numerical simulation and the experiments can be found in fig. 3.

3.1 Experimental Results

At first the 10-minute averages of the lidar measured wind speed component v_r and the 3D sonic wind vector projected on the line-of-sight, $\boldsymbol{n} \cdot \boldsymbol{u}$, have been compared. A filter has been applied for radial components less than 2 ms, because it is not possible to accurately determine v_r below that value for a homodyne lidar system. The comparison can be seen in fig. 4. For both beams a very good comparison can be observed; the line fits yield slopes of unity and an R^2 of almost 100%. The line fits for the other methods can be found in tab. 1. The difference between the methods is negligible. An example of a time series result can be found in fig. 3.

Atmos. Meas. Tech. Discuss., https://doi.org/10.5194/amt-2018-229
Manuscript under review for journal Atmos. Meas. Tech.
Discussion started: 13 August 2018

Figure 2. *Left*: Photo depicting the lidar mounted on the mast looking at the two sonic anemometers, Dellwik et al. (2015). *Right*: Google Earth screen shot of the site setup

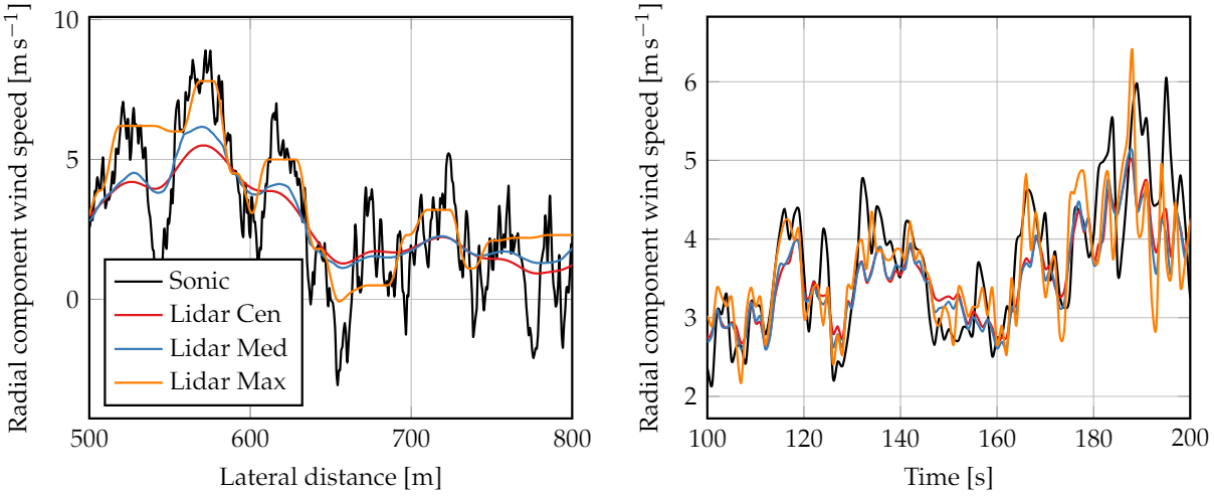

Figure 3. Example data for the numerical simulation (*left*) and the experiment (*right*).

Table 1. Parameters of the line fit to the 10-minute correlation between sonic radial component and lidar.

	Centroid		Median		Maximum	
	line fit	R^2 [%]	line fit	R^2 [%]	line fit	R^2 [%]
North	$1.001x - 0.040$	99.42	$1.001x - 0.021$	99.48	$0.999x - 0.051$	99.00
South	$1.003x - 0.028$	99.55	$1.003x - 0.008$	99.59	$1.001x - 0.039$	99.06

Atmos. Meas. Tech. Discuss., https://doi.org/10.5194/amt-2018-229
Manuscript under review for journal Atmos. Meas. Tech.
Discussion started: 13 August 2018

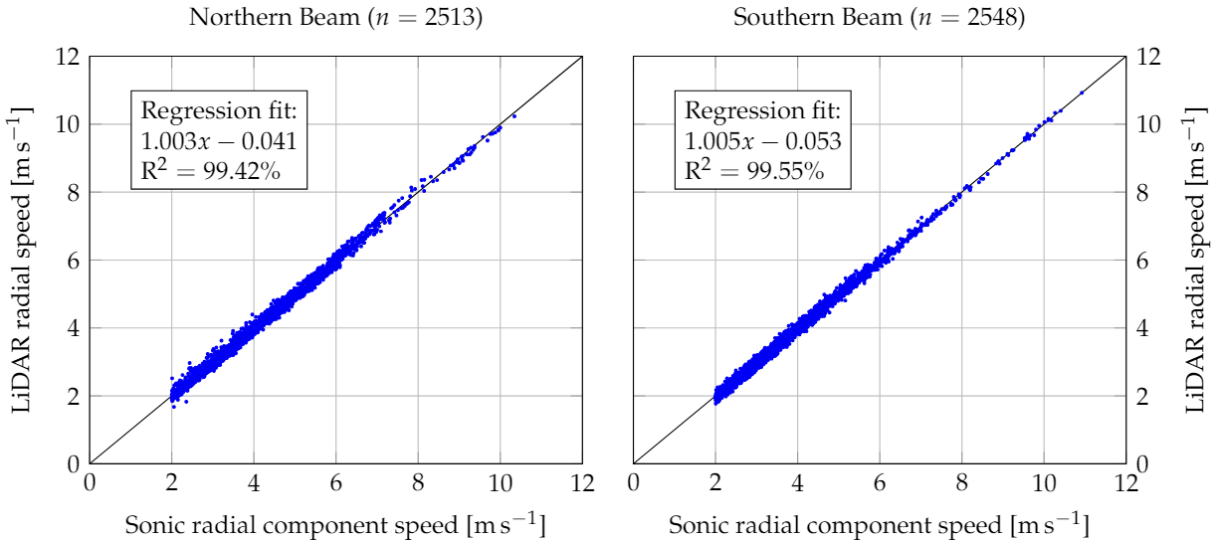

Figure 4. 10-minute average sonic radial component speed versus lidar wind speed. The lidar wind speed has been calculated using the centroid method.

For wind lidar systems using a homodyne detection method there exists an ambiguity in wind direction (whether the wind blows towards or away from the lidar) and in misalignment (whether the wind direction is misaligned towards the left or right side of the beam); the radial wind speed measurements will be the same. For example, a case of a wind direction misaligned by $10°$ is equivalent to a misalignment of $170°$, $190°$ and $350°$. Thus, it is possible to reduce the full $360°$ to one quadrant ranging from $0°$ to $90°$. For the two beams this is shown in fig. 5, where the data is binned into bins of $10°$ width. It can be seen that the data is spread rather evenly over the sectors, but sectors close to $90°$ show no data since in these cases the laser beam and wind direction are perpendicular and the radial speed component is very close to zero.

To create numerical simulations as close as possible to the experimental conditions, the Mann spectral tensor has been fitted to the u and v spectra obtained from sonic measurements, where the mean wind speed was above 6 ms^{-1}. The tensor model has three parameters: $\alpha\epsilon^{2/3}$ where ϵ is the rate of viscous dissipation of turbulent kinetic energy and α the spectral Kolmogorov constant, L is a length scale and Γ is an anisotropy parameter, for details see Mann (1994). This has been done sector-wise for each beam and the results can be seen in tab. 2.

In order to reduce the computational effort we have taken the average value of each parameter over all sectors and both beams and found the following parameter: $\alpha\epsilon^{\frac{2}{3}} = 0.58 \cdot 10^{-2}\text{m}^{4/3}\text{s}^{-2}$, $L = 22.3\,\text{m}$, $\Gamma = 2.26$. These parameters have been used to perform the numerical simulations mentioned in section 2.2.

Atmos. Meas. Tech. Discuss., https://doi.org/10.5194/amt-2018-229
Manuscript under review for journal Atmos. Meas. Tech.
Discussion started: 13 August 2018

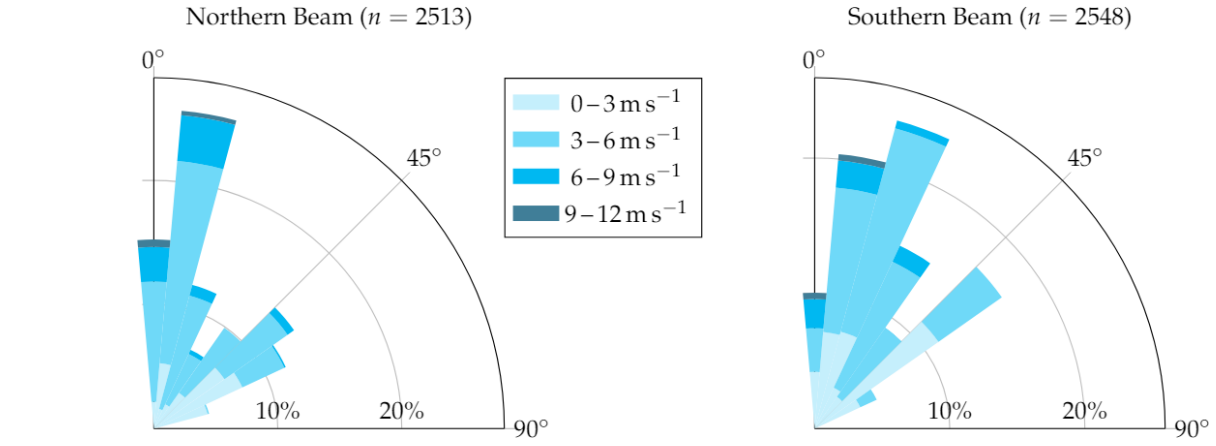

Figure 5. Difference of wind direction to the northern beam (*left*) and southern beam (*right*) reduced to the first quadrant due to the homodyne detection agnostic to direction sensing.

Table 2. Sectorwise fitted parameters of the Mann model for each beam.

Misalignment		0°	10°	20°	30°	40°	50°	60°	70°	80°	90°
North	$10^{-2}\alpha\epsilon^{\frac{2}{3}}$ [m$^{4/3}$s^{-2}]	1.11	1.02	1.14	0.38	0.37	0.26	0.32	0.41	-	-
	L [m]	5.1	7.5	10.4	19.0	26.3	28.3	28.3	35.3	-	-
	$\Gamma[-]$	3.33	2.49	2.03	1.94	1.97	2.35	1.88	1.77	-	-
South	$10^{-2}\alpha\epsilon^{\frac{2}{3}}$ [m$^{4/3}$s^{-2}]	0.61	0.65	0.90	0.40	0.39	0.32	0.35	-	-	-
	L [m]	19.9	14.8	7.1	36.5	42.1	31.1	22.8	-	-	-
	$\Gamma[-]$	1.85	2.43	3.31	1.60	1.87	2.32	2.79	-	-	-

3.2 Combined results

In this section we will present the combination of experimental and simulation results together with the numerical integration of eq. 2 (using eq. 3 - 5). In the following plots theoretical results are represented by a solid black line, simulation results (*Simu*) are indicated by coloured solid lines and experimental results (*Exp*) by coloured dashed lines. The different colors stand for the three methods to derive the radial speed from the Doppler spectrum: centroid (*cen*), median (*med*) and maximum (*max*).

First, we present the simplest case when the lidar beam is aligned with the wind direction. In this case eq. 2 can be solved analytically because the exponential in eq. 3 and 5 does not depend on either k_2 or k_3 and can be moved outside the integral. This results in

$$G(k_1) = \left|\frac{\chi_{r,s}(k_1)}{F_s(k_1)}\right|^2 = \left|\frac{\exp\left(-z_R|\boldsymbol{n}\cdot\boldsymbol{k}|\right)\int_{-\infty}^{+\infty}\int_{-\infty}^{+\infty}\boldsymbol{\Phi}_{i,j}(\boldsymbol{k})dk_2dk_3}{\int_{-\infty}^{+\infty}\int_{-\infty}^{+\infty}\boldsymbol{\Phi}_{i,j}(\boldsymbol{k})dk_2dk_3}\right|^2 = \exp\left(-2z_Rk_1\right). \tag{10}$$

Note that in eq. 10 the radial speed is defined by the centroid method.

Atmos. Meas. Tech. Discuss., https://doi.org/10.5194/amt-2018-229
Manuscript under review for journal Atmos. Meas. Tech.
Discussion started: 13 August 2018

Atmospheric Measurement Techniques Discussions

The results for the aligned case is shown in fig. 6, where eq. 10 is shown as the black solid line. It can be seen that both red lines (solid and dashed) agree well with the theoretical results. Some significant deviations can be observed for the simulation results at small wave numbers, which can be explained by the truncation of the Doppler spectrum in eq. 9.

It can also be seen that the transfer function when using the median or maximum method lie above the results for the centroid method. This indicates that fluctuations which have been measured by the sonic and are attenuated when using the centroid method due to volume averaging can indeed be seen when using the median and maximum method. The median method seems to be slightly better than the centroid method and the maximum method has an even bigger improvement.

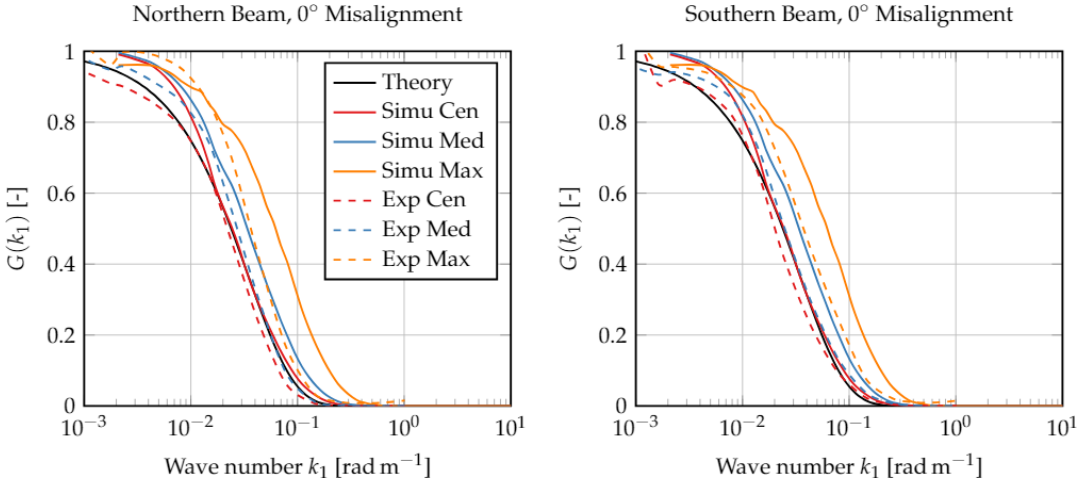

Figure 6. Transfer function $G(k_1)$ for aligned beams for the northern beam data (*left*) and southern beam data (*right*).

As an example for a misaligned case, we will now focus on a misalignment of $40°$, see fig. 7. The transfer functions for the remaining misalignments can be found in the appendix. For a misalignment of $40°$ eq. 10 is not valid anymore. However, eq. 2 can be integrated numerically. It is shown again as the solid black line. Again we can see that the simulation results using the centroid method matches the theoretical results well for large wave numbers, but there are deviations at low wave numbers. Also the previous observation of improved transfer functions for the median and maximum method is noticed again.

Examples of these improvements can also be identified in time domain when looking at fig. 3. For the numerical simulations (left panel) the improved fluctuation measurements using the maximum method are very clear, while the median method is also able to slightly enhance the measurements compared to the centroid method, which performs worst. A similar tendency is also observed from the experiment (right panel). Just before 120 s we can note a very good agreement between sonic and maximum-method v_r, whereas the other two methods can not detect this fluctuation. In other periods the observed improvement is very small.

Next we consider the RMSE results. Since it was seen previously that both the median and maximum method outperformed the centroid method, the RMSE of the two methods normalized by the RMSE of the centroid is compared now

$$1 - \mathrm{RMSE}(v_{r,\mathrm{method}})/\mathrm{RMSE}(v_{r,\mathrm{cen}}), \tag{11}$$

Atmos. Meas. Tech. Discuss., https://doi.org/10.5194/amt-2018-229
Manuscript under review for journal Atmos. Meas. Tech.
Discussion started: 13 August 2018

Atmospheric Measurement Techniques Discussions

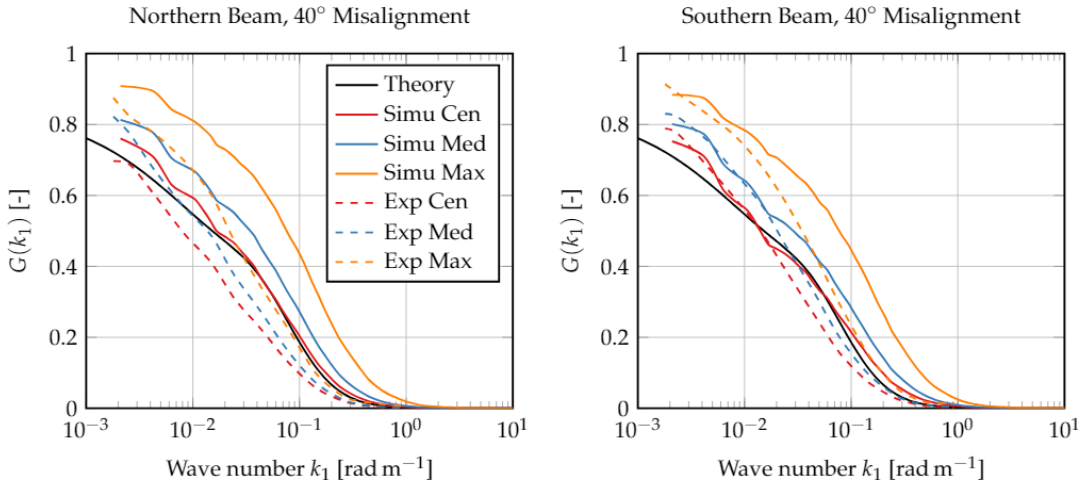

Figure 7. Transfer function $G(k_1)$ for misaligned beams for the northern beam data (*left*) and southern beam data (*right*).

where method is either the median or the maximum method. Thus positive numbers indicate better performance compared to the centroid method and vice versa.

The results can be seen in fig. 8 and show that the median method consistently outperforms the centroid method. Improvements of up to 4% from the experimental data was observed, while the simulations showed performance increase between 3 to 5%.

In contrast, the maximum method has persistent disadvantages compared to the centroid method. The shortcoming increases with increasing misalignment and reaches values of approximately -9% for the experiments and close to -10% for the numerical simulations. This indicates that the improved performance of the maximum method in reducing the effect of spatial averaging has the consequence that more signal noise is introduced due to the discretisation of selecting the maximum of the Doppler spectrum.

4 Conclusions

In this study we compared cw wind lidar to sonic measurements, where the sonic anemometers are mounted exactly at the focus positions of the lidar system. The objective of the paper was to study how different methods of determining the dominant frequency in a Doppler spectrum affect wind speed measurements by a cw lidar. We used an estimation of the transfer function to evaluate the lidar's attenuation of turbulent fluctuations due to its large measurement volume and the RMSE to give a metric to the general performance of the methods. Theoretical analysis, numerical simulation and data from a two-month long experiment have been used and three different methods for deriving the radial speed were applied: the centroid, median and maximum method.

The analysis was able to show that the simulations as well as the experiments agree well with the theoretical results for the centroid method. Further, the median and maximum method performed better both in simulation and experiment compared to

Atmos. Meas. Tech. Discuss., https://doi.org/10.5194/amt-2018-229
Manuscript under review for journal Atmos. Meas. Tech.
Discussion started: 13 August 2018

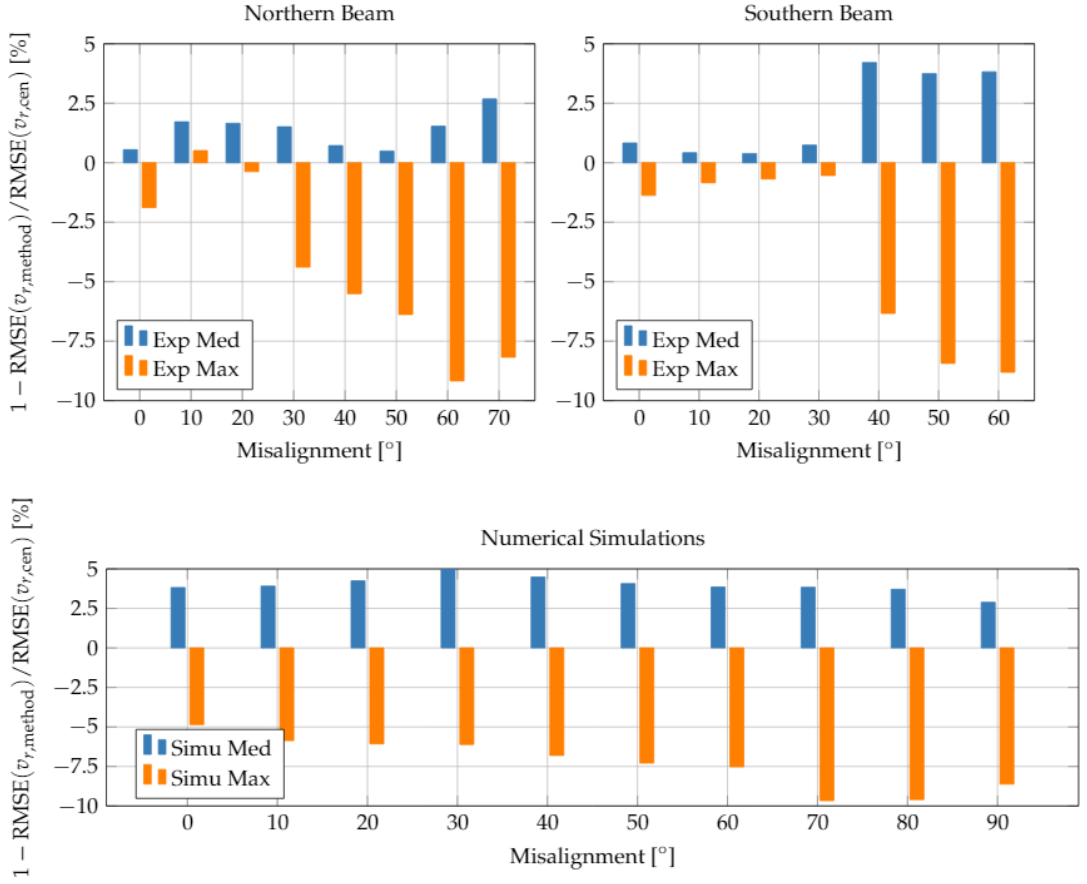

Figure 8. RMSE value for the median and maximum method normalised by RMSE($v_{r,\mathrm{cen}}$) for the experimental results (*top*) and the numerical simulations (*bottom*).

the centroid method in reducing the effect of spatial averaging. Interestingly the maximum method had the highest reduction. However, it also showed the highest RMSE values out of all methods due to the discretisation of picking the maximum value of the Doppler spectrum. Thus, from this study we conclude that if one's aim is to retrieve point-like time series with a high effective sampling rate, the median method can improve the results and reduce the effect of spatial averaging. When comparing 10 minute averages all methods performed equally well.

The method of using average Doppler spectra (typically 10 or 30 minute averages) has also been studied to derive turbulence statistics (Branlard et al., 2013). However, using this approach only statistics can be derived, namely the wind speed PDF and its statistical moments. What is presented here shows how carefully choosing the method of radial speed retrieval from a Doppler spectrum can partly alleviate the inherent volume averaging effect of lidar systems for a complete time series.

It should be noted that these conclusions only apply to cw lidars and not to pulsed systems as the method of deriving radial velocities is different for the latter.

Atmos. Meas. Tech. Discuss., https://doi.org/10.5194/amt-2018-229
Manuscript under review for journal Atmos. Meas. Tech.
Discussion started: 13 August 2018

Atmospheric Measurement Techniques Discussions

Code and data availability. The computer code to generate synthetic turbulence fields can be found at: http://www.wasp.dk/weng#details_ _iec-turbulence-simulator. The data is available at

Appendix A: Transfer Functions for the Remaining Misalignment Directions

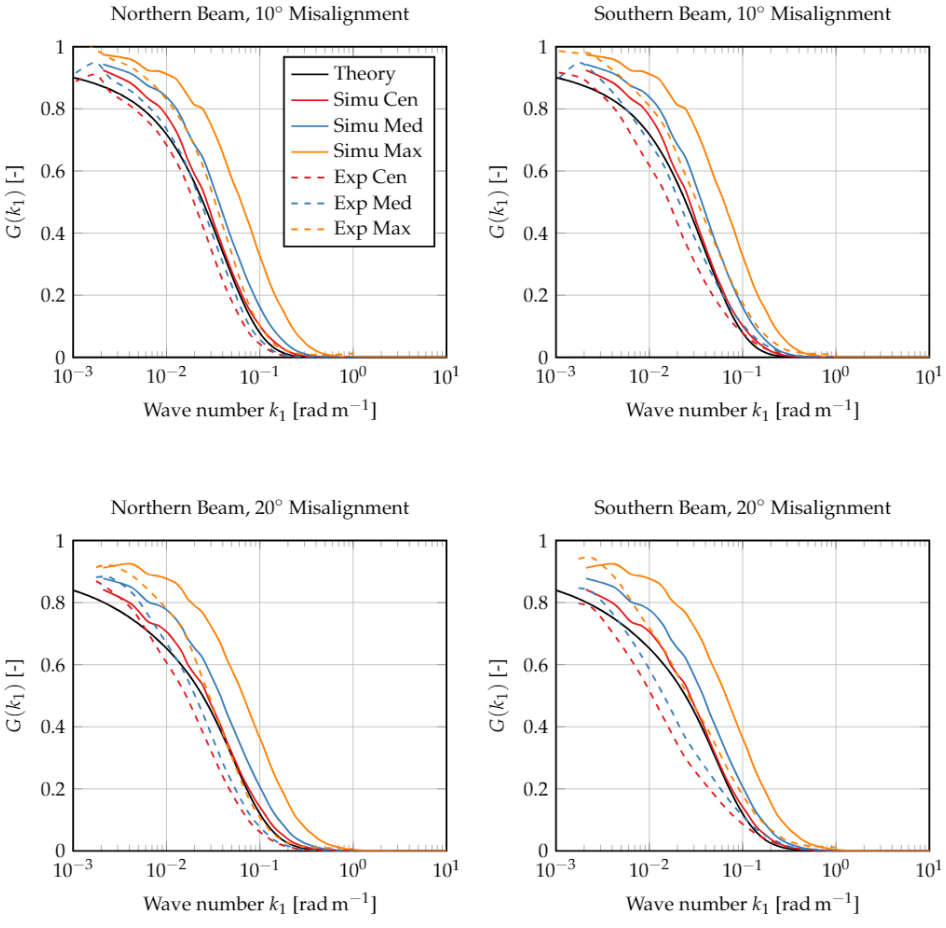

Author contributions. Dominique P Held performed the research work and prepared the manuscript. Jakob Mann conceived the reserach plan, supervised the research work and the manuscript preparation.

Competing interests. The work of Dominique P Held was partly funded by Windar Photonics A/S through an industrial PhD stipend (project number: 5016-00182).

Atmos. Meas. Tech. Discuss., https://doi.org/10.5194/amt-2018-229
Manuscript under review for journal Atmos. Meas. Tech.
Discussion started: 13 August 2018

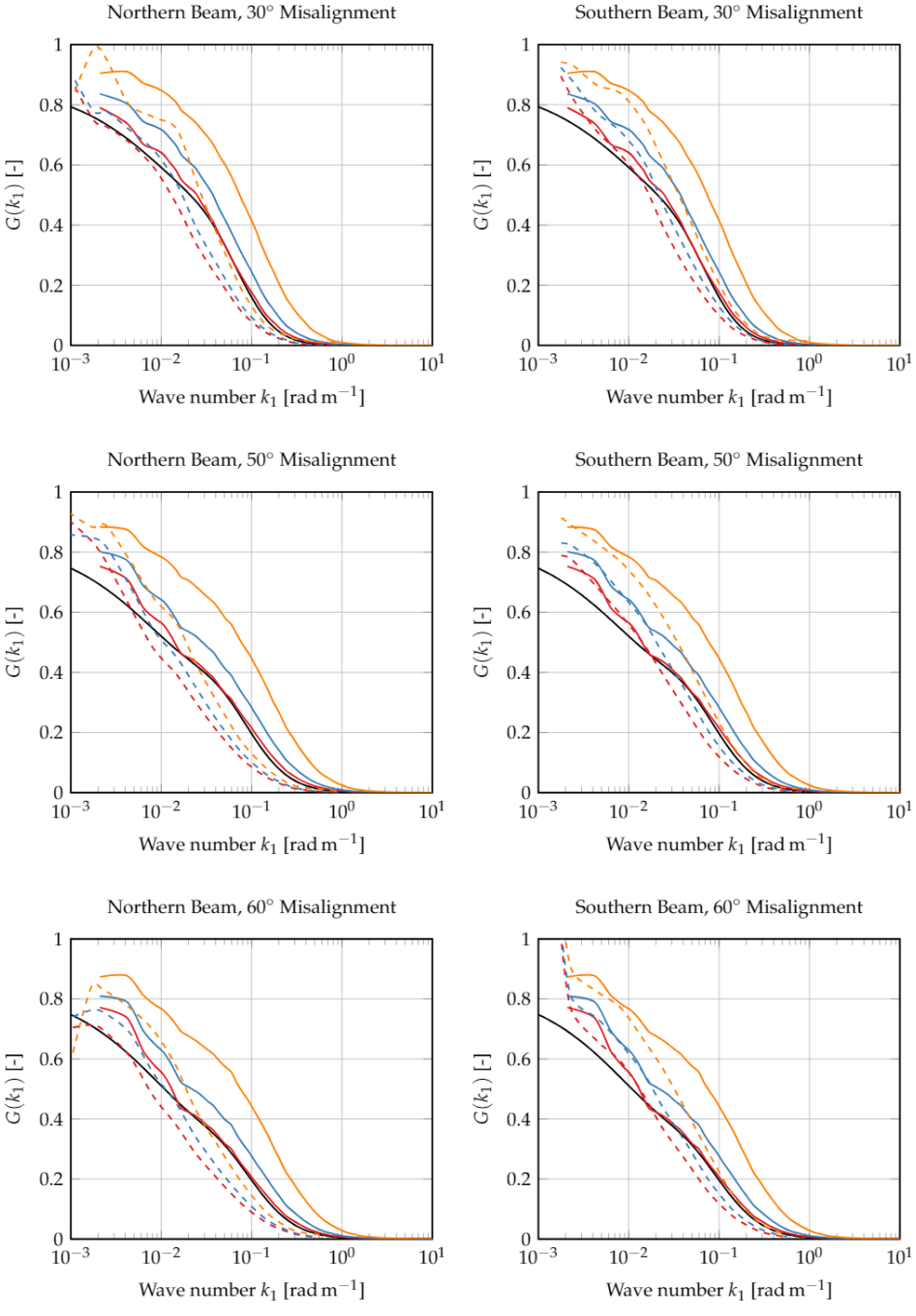

Acknowledgements. This study was supported by Innovationsfonden Danmark in form of an industrial PhD stipend (project number: 5016-00182). The authors want to thank Ebba Dellwik and Antoine Larvol for their support with the sonic anemometer and LiDAR data.

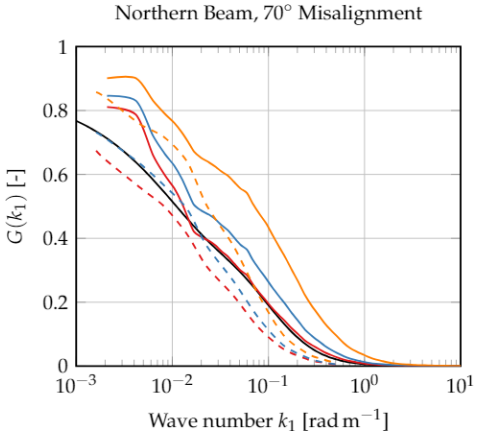

References

Angelou, N., Mann, J., Sjöholm, M., and Courtney, M. S.: Direct measurement of the spectral transfer function of a laser based anemometer, Review of Scientific Instruments, 83, https://doi.org/10.1063/1.3697728, 2012.

Banakh, V. A. and Smalikho, I. N.: Measurements of turbulent energy dissipation rate with a CW Doppler lidar in the atmospheric boundary layer, Journal of Atmospheric and Oceanic Technology, 16, 1044–1061, https://doi.org/10.1175/1520-0426(1999)016<1044:MOTEDR>2.0.CO;2, http://journals.ametsoc.org/doi/abs/10.1175/1520-0426(1999)016%3C1044:MOTEDR%3E2.0.CO;2, 1999.

Bechmann, A., Berg, J., Courtney, M. S., Jørgensen, H. E., Mann, J., and Sørensen, N. N.: The Bolund Experiment: Overview and Background, Tech. rep., DTU, http://orbit.dtu.dk/fedora/objects/orbit:81901/datastreams/file_4321515/content, 2009.

Borraccino, A., Courtney, M. S., and Wagner, R.: Generic Methodology for Field Calibration of Nacelle-Based Wind Lidars, Remote Sensing, 8, 907, https://doi.org/10.3390/rs8110907, http://www.mdpi.com/2072-4292/8/11/907, 2016.

Borraccino, A., Courtney, M. S., and Wagner, R.: Remotely measuring the wind using turbine-mounted lidars: Application to power performance testing, Ph.D. thesis, Technical University of Denmark, https://doi.org/10.11581/DTU, 2017.

Branlard, E., Pedersen, A. T., Mann, J., Angelou, N., Fischer, A., Mikkelsen, T., Harris, M., Slinger, C., and Montes, B. F.: Retrieving wind statistics from average spectrum of continuous-wave lidar, Atmospheric Measurement Techniques, 6, 1673–1683, https://doi.org/10.5194/amt-6-1673-2013, 2013.

Dellwik, E., Sjöholm, M., and Mann, J.: An evaluation of the WindEye wind lidar, Tech. rep., Technical University of Denmark, 2015.

Dolfi-Bouteyre, A., Canat, G., Lombard, L., Valla, M., Durécu, A., and Besson, C.: Long-range wind monitoring in real time with optimized coherent lidar, Optical Engineering, 56, 031 217, https://doi.org/10.1117/1.OE.56.3.031217, http://opticalengineering.spiedigitallibrary.org/article.aspx?doi=10.1117/1.OE.56.3.031217, 2016.

Frehlich, R.: Scanning doppler lidar for input into short-term wind power forecasts, Journal of Atmospheric and Oceanic Technology, 30, 230–244, https://doi.org/10.1175/JTECH-D-11-00117.1, 2013.

Fuertes, F. C., Iungo, G. V., and Porté-Agel, F.: 3D turbulence measurements using three synchronous wind lidars: Validation against sonic anemometry, Journal of Atmospheric and Oceanic Technology, 31, 1549–1556, https://doi.org/10.1175/JTECH-D-13-00206.1, 2014.

Harris, M., Hand, M., and Wright, A. D.: Lidar for turbine control, Tech. rep., NREL, https://doi.org/NREL/TP-500-39154, http://gisceu.net/PDF/U373.pdf, 2006.

Hu, Q.: Semiconductor Laser Wind Lidar for Turbine Control, Ph.D. thesis, Technical University of Denmark, 2016.

Kristensen, L. and Jensen, N. O.: Lateral coherence in isotropic turbulence and in the natural wind, Boundary-Layer Meteorology, 17, 353–373, https://doi.org/10.1007/BF00117924, 1979.

Lawrence, T. R., Wilson, D. J., Craven, C. E., Jones, I. P., Huffaker, R. M., and Thomson, J. A. L.: A laser velocimeter for remote wind sensing, Review of Scientific Instruments, 43, 512–518, https://doi.org/10.1063/1.1685674, 1972.

Mann, J.: The spatial structure of neutral atmospheric surface-layer turbulence, Journal of Fluid Mechanics, 273, 141–168, https://doi.org/10.1017/S0022112094001886, 1994.

Mann, J., Cariou, J. P., Courtney, M. S., Parmentier, R., Mikkelsen, T., Wagner, R., Lindelöw, P., Sjöholm, M., and Enevoldsen, K.: Comparison of 3D turbulence measurements using three staring wind lidars and a sonic anemometer, Meteorologische Zeitschrift, 18, 135–140, https://doi.org/10.1127/0941-2948/2009/0370, 2009.

Mann, J., Peña, A., Bingöl, F., Wagner, R., and Courtney, M. S.: Lidar Scanning of Momentum Flux in and above the Atmospheric Surface Layer, Journal of Atmospheric and Oceanic Technology, 27, 959–976, https://doi.org/10.1175/2010JTECHA1389.1, http://journals.ametsoc.org/doi/abs/10.1175/2010JTECHA1389.1, 2010.

Newman, J. F. and Clifton, A.: An error reduction algorithm to improve lidar turbulence estimates for wind energy, Wind Energ. Sci, 2, 77–95, https://doi.org/10.5194/wes-2-77-2017, www.wind-energ-sci.net/2/77/2017/, 2017.

Pauscher, L., Vasiljevic, N., Callies, D., Lea, G., Mann, J., Klaas, T., Hieronimus, J., Gottschall, J., Schwesig, A., Kühn, M., and Courtney, M.: An Inter-Comparison Study of Multi- and DBS Lidar Measurements in Complex Terrain, Remote Sensing, 8, 782, https://doi.org/10.3390/rs8090782, http://orbit.dtu.dk/ws/files/127594944/An_Inter_Comparison_Study.pdf, 2016.

Peña, A., Mann, J., and Dimitrov, N.: Turbulence characterization from a forward-looking nacelle lidar, Wind Energy Science, 2, 133–152, https://doi.org/10.5194/wes-2-133-2017, https://www.wind-energ-sci.net/2/133/2017/, 2017.

Sanz Rodrigo, J., Borbón Guillén, F., Gómez Arranz, P., Courtney, M. S., Wagner, R., and Dupont, E.: Multi-site testing and evaluation of remote sensing instruments for wind energy applications, Renewable Energy, 53, 200–210, https://doi.org/10.1016/j.renene.2012.11.020, http://dx.doi.org/10.1016/j.renene.2012.11.020, 2013.

Schlipf, D.: Lidar-Assisted Control Concepts for Wind Turbines, Ph.D. thesis, University of Stuttgart, 2015.

Sjöholm, M., Mikkelsen, T., Mann, J., Enevoldsen, K., and Courtney, M. S.: Spatial averaging-effects on turbulence measured by a continuous-wave coherent lidar, Meteorologische Zeitschrift, 18, 281–287, https://doi.org/10.1127/0941-2948/2009/0379, 2009.

Sonnenschein, C. M. and Horrigan, F. A.: Signal-to-Noise Relationships for Coaxial Systems that Heterodyne Backscatter from the Atmosphere., Applied Optics, 10, 1600–4, https://doi.org/10.1364/AO.10.001600, http://www.ncbi.nlm.nih.gov/pubmed/20111170, 1971.

von Karman, T.: Progress in the Statistical Theory of Turbulence, Proceedings of the National Academy of Sciences, 34, 530–539, http://www.pnas.org.proxy.findit.dtu.dk/content/34/11/530, 1948.